Electron capture in low-energy collisions of C^{q+} and O^{q+} with H and H_2

R. A. Phaneuf, I. Alvarez,* F. W. Meyer, and D. H. Crandall
Oak Ridge National Laboratory, Oak Ridge, Tennessee 37830
(Received 14 May 1982)

Total electron-capture cross-section measurements are reported for C^{q+} $(3 \leq q \leq 6)$ and O^{q+} $(2 \leq q \leq 6)$ ions colliding with hydrogen atoms and molecules in the energy range $(0.01 \leq E \leq 10)$ keV/amu. The cross sections range from $(0.5-7)\times 10^{-15}$ cm^2, and neither obey simple charge-scaling rules, nor exhibit uniform dependences on collision velocity in this energy range. For a given charge q, cross sections for the less-highly-stripped oxygen ions exceed those for carbon ions at energies below a few-hundred eV/amu. Comparison is made between these measurements and theoretical calculations which have heretofore remained untested at low collision energies. In general, the agreement is good for those systems where detailed perturbed-stationary-state theory is available, but is best with those calculations in which the collision dynamics as well as the molecular couplings are treated quantum mechanically. Generalized theories which work well for collision systems containing many bound electrons, do not give accurate representations of these few-electron systems at low energies.

I. INTRODUCTION

The inelastic process whereby a multiply ionized ion captures an electron from a neutral atom has received considerable theoretical and experimental attention in recent years. Cross sections for such processes are typically large ($> 10^{-15}$ cm^2), and hence charge exchange is often the dominant inelastic process in environments containing both highly charged ions and neutrals. In astrophysics, charge transfer in slow collisions with hydrogen and helium is important in reducing the degree of ionization of highly charged ions in the photon-ionized interstellar gas.[1,2] Charge-changing collisions between highly ionized impurities and hydrogen isotopes also strongly affect the ionization balance in magnetically confined thermonuclear fusion plasmas.[3–5] The penetration and energy deposition of injected neutral beams,[4] the transport and recycling of impurities in the plasma,[5] and the interpretation of diagnostic measurements[5–7] all are affected to varying degrees by the charge-exchange process. Charge-exchange recombination must also be considered in the design, modeling, and operation of multicharged ion sources.[8]

Theoretical research on low-energy electron-capture collisions of multicharged ions has evolved in two directions: approximate or generalized estimates which may be applied to a wide variety of systems, and detailed calculations for specific collision partners. In the present context, a low velocity collision refers to one in which the nuclear motion is slow compared to the motion of the bound electron being captured. Under such conditions, the electrons have sufficient time to adjust to the changing interatomic field as the nuclei approach and separate, and a quasimolecular description of the collision becomes necessary for a detailed treatment of the problem. The electron-capture process is represented as a transition between the stationary states of the quasimolecule. Predicted cross sections depend strongly on the internuclear distance at which the potential energy curves have minimum separation, or "cross," and on the dynamics of the coupling between the stationary states.

For multielectron systems involving highly stripped ions colliding with complex targets, or partially stripped heavy ions colliding with simple one-electron targets, the number of such "curve crossings" which are possible during the collision is large, and generalized theoretical models[9–12] become quite reliable. In such systems, the cross sections are predicted to be large, insensitive to collision velocity, and to scale smoothly with ionic charge. Such predictions have been verified experimentally for noble-gas ions colliding with noble gases,[13–15] for Ar and Xe ions with atomic and molecular hydrogen,[16] and for Ar ions colliding with molecular deuterium.[17]

The collision of a highly stripped or bare ion with a one-electron atom presents a somewhat different

physical situation. Usually one or at most a few curve crossings exist which are favorable for electron capture. In this case both the magnitude and velocity dependence of the cross section depend on the details of the potential energy curves representing that particular quasimolecule and on the couplings between them.[18] Most of the development of perturbed-stationary-state (PSS) theory for multiply charged ions has focused on the simplest possible case, the one-electron diatomic system, where a bare nucleus collides with a ground-state hydrogen atom.[19–24] The majority of these calculations have been performed within an impact-parameter formalism in which the nuclear motion is treated classically. The breakdown of this method at the very lowest energies has stimulated the recent development of a fully quantal approach[25,26] which is particularly applicable in situations of interest in astrophysics. In the interstellar medium the high charge states of the ions are produced by successive photoionization, and the degree of electronic excitation is very large relative to the kinetic energy of the ions.

Another approach which has met with considerable success is the application of the unitarized distorted-wave approximation based on atomic orbitals.[27] While this method is applicable over the broadest energy range of any of the theoretical approaches, it becomes decreasingly reliable at collision energies below several hundred eV/amu, where a molecular treatment is indicated.

The evaluation of the perturbed-stationary-state calculations, and the various approximations which have been applied to make them more tenable, requires measurements of cross sections for electron capture by nearly or fully stripped ions colliding with atomic hydrogen at low energies. The lack of any experimental data for such collisions is a consequence of the difficulty of extracting ion beams in high charge states from multicharged ion sources at energies below 1 keV/amu. In the experiments reported here, advantage is taken of the unique properties of a pulsed-laser-produced plasma for this application. Such a plasma is characterized by a very high degree of ionization relative to ion kinetic energy. Heating of the electrons and ions is facilitated by inertial confinement of the high-density plasma, rather than by the use of external fields, as is the case in more conventional multicharged ion sources.[8]

In this paper, experimental cross sections are reported for C^{q+} $(3 \leq q \leq 6)$ and O^{q+} $(2 \leq q \leq 6)$ colliding with H and H_2 at energies ranging from 11 eV/amu for C^{3+} to 10 keV/amu for O^{6+}. Some of the C^{q+} data reported here have been published previously in a brief communication.[28] The present measurements are believed to be the first reported electron-capture cross-section data for either nearly or fully stripped ions colliding with atomic hydrogen at energies below 1 keV/amu.

II. EXPERIMENTAL METHOD

The present data were obtained by directing a collimated beam of multiply charged ions of charge q through a calibrated atomic- or molecular-hydrogen gas target, and detecting scattered product ions of charge $q-1$ separately from the primary ions of charge q. Cross-section measurements at energies in the 0.4- to 10-keV/amu range were obtained using ion beams produced in the ORNL-PIG multicharged ion source. In these experiments the ions were charge analyzed after the collision by electrostatic deflection. The apparatus, experimental technique, and evaluation of systematic effects have all been described in detail[16,29] and will not be reiterated here. Ion beams for the lower energy data were obtained from an expanding laser-produced plasma. Bursts of collimated and energy-selected ions were directed through the atomic- or molecular-hydrogen gas target and analyzed by a time-of-flight technique. The apparatus and experimental technique have been reported briefly elsewhere[28,30] and will be more fully described in another paper. We present here only those experimental details which bear directly upon the reported cross-section measurements, and on the uncertainties associated with them.

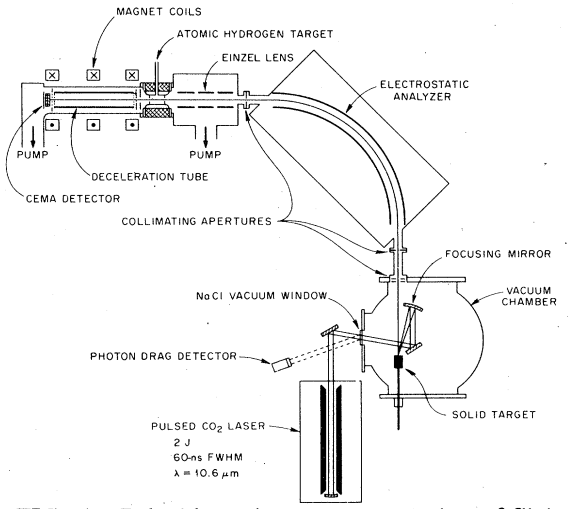

FIG. 1. Pulsed-laser ion source and time-of-flight electron-capture collision apparatus.

A. General method

The arrangement of the laser-ion-source and associated time-of-flight apparatus is shown in Fig. 1. The principle of measurement is similar to that reported previously by Goldhar and co-workers,[31] who measured cross sections for electron capture in noble gases by highly stripped carbon ions from a laser-produced plasma. Modifications were made in several areas in order to increase the accuracy and extend the applicability of the experimental method. The major changes involve the post-collision charge analysis, the ion detector, the data acquisition system, and the incorporation of a thermal-dissociation atomic-hydrogen gas target.

A dense plasma is created by focusing a 3-J pulse of 10.6-μm radiation from a TEA-CO_2 laser onto a graphite or ThO_2 target in vacuum to a power density of $\sim 3\times 10^{10}$ W/cm^2. Since the goal of this investigation was the measurement of electron-capture cross sections for highly stripped ions at the lowest attainable energies, no provision was made for the extraction and acceleration of ions from this plasma. A series of apertures simply collimate a beam from the expanding plasma and a cylindrical electrostatic analyzer selects ions having a fixed energy per charge (E/q) determined by the voltage on the plates. Ions emerging from the analyzer are focused by an einzel lens through a differentially pumped atomic-hydrogen gas target cell, passed through a gridded deceleration tube, and are detected by a channel electron multiplier array (CEMA) detector. Three coils provide an axial magnetic field of up to 0.05T, which collimates the ion beam, offsetting beam blowup in the deceleration tube, and assuring detection of all ions which enter the collision cell. The total path length from the laser target to the ion detector is 260 cm, and typical ion flight times range from 5 to 50 μs.

A photon detector samples a small fraction of the laser light reflected by the NaCl vacuum window, providing an accurate timing pulse. The time-of-flight ion current signals from the CEMA detector are recorded by a 1024-channel transient digitizer having a resolution of 8 bits at 50 ns/channel. A microprocesser controls the firing of the laser, the pulsing of the magnet coils, and averages successive time-of-flight spectra. A typical signal measurement involved an average over 50 laser shots at a repetition rate of 0.2 Hz.

B. Time-of-flight analysis

The separation of the various ion charge states by time-of-flight is based on the fact that the laser-produced plasma is short lived relative to ion flight times in the apparatus, and that an electrostatic energy analyzer transmits to the exit aperture only ions of a selected energy per charge (E/q). Hence for a given voltage on the analyzer plates, each charge q will arrive at the detector at a different time t, such that $t \propto (m/q)^{1/2}$. The deceleration charge-exchange analyzer takes advantage of the fact that an ion of a selected E/q that subsequently captures an electron has energy per charge $E/(q-1)$, and is thus retarded less by electrostatic deceleration. The required retarding voltage relative to E/q depends both on the ionic charge and on the energy resolution of the analyzer, which was typically 2% for these measurements. The einzel lens allowed ions emerging from the analyzer into a variable solid angle to be directed through the gas target cell, and thus permitted a trade-off between ion intensity and energy resolution. However, great care was taken to ensure that the angular divergence of the ion beam produced in this manner was well within the acceptance of the target cell and detector. This is further discussed in Sec. III. Time-of-flight spectra illustrating the technique for cross-section measurement are shown in Fig. 2 for 1032-eV/q oxygen ions passing through an atomic-

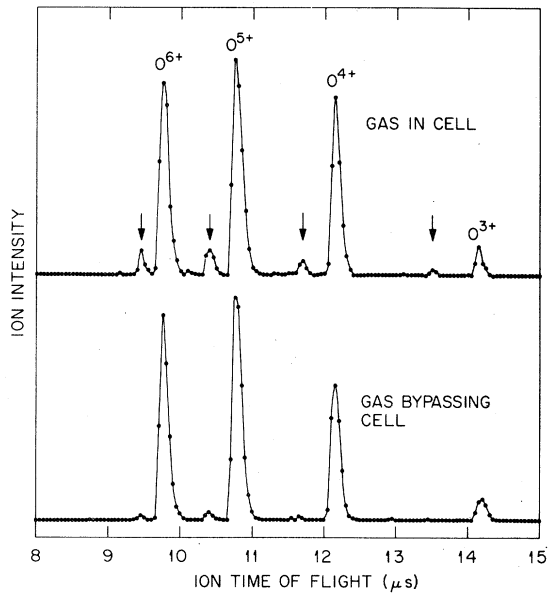

FIG. 2. Digitized time-of-flight ion intensity spectra for oxygen ions at 1032 eV/charge, with + 700 V on deceleration charge analyzer. Ions which have captured an electron are delayed less than the primary ions and are designated by arrows. Particle density in the atomic-hydrogen collision cell is 6×10^{12} cm^{-3}. Spectra are averages over 100 laser shots.

hydrogen target. At the maximum focused laser power density of 3×10^{10} W/cm^2, O^{7+} ions were detected on some shots, but their number was insufficient for cross-section measurements. The fact that usable fluxes of C^{6+} nuclei were obtained, whereas H-like O^{7+} ions were not, is due to the significantly larger ionization potential of O^{6+} (839 eV) relative to that for C^{5+} (489 eV).

C. Ion detector

Several characteristics of the chevron CEMA made it an appropriate choice for the present application. The large active area (2.5 cm diam) allowed the entire beam to be detected despite significant beam blowup in the deceleration tube. The application of an axial magnetic field to counteract this blowup had no measurable effect on the detector response. The pulsed nature of the laser source resulted in typical fluxes of several hundred ions arriving within fractions of a microsecond. Thus the CEMA was used as a current amplifier, rather than in a single-particle counting mode, and, provided the gain was kept at 10^6 or lower, the response was determined to be linear even at these large particle arrival rates. This is presumably due to the multipore construction of the detector, its finite capacitance, and the large extent of the impinging beam relative to the pore diameter (12 μm). A fine 98% transmitting copper-wire grid was placed in front of the CEMA, and the grid and CEMA front surface were typically operated at -2 kV in order to accelerate the ions and thereby increase the sensitivity of the low-energy ions. The grid serves to make the response more uniform across the CEMA surface when the latter is operated at high voltage.[32] Ion-impact energies ranged from 6 to 14 keV. The detector bias circuit was arranged such that the potential on the front face could be varied, while the voltage drop across the device, and therefore the gain, was held constant. This enabled the variation of sensitivity with ion impact velocity to be measured *in situ* under actual experimental conditions. Such measurements and relative corrections for variation of detector sensitivity with ionic charge for ions of the same velocity are discussed in Sec. III.

D. Atomic-hydrogen target and calibration

The ORNL atomic-hydrogen gas target and the procedures employed for its calibration have been discussed in detail in reports on previous work.[29,33] The thin cylindrical tungsten tube, 0.6 cm in diameter and 2.5 cm long, is heated to 2350 K by passing a direct current of 130 A through it. For the present data taken with the ORNL-PIG ion source, the oven tube and calibration were exactly as previously reported.[29,33] For the experiments with ions from the laser source, a new tungsten tube was fabricated, having 0.1- and 0.2-cm-diam entrance and exit apertures, respectively. As in previous work, the target-thickness calibration and the dissociation fraction were determined prior to the measurements in an auxiliary experiment using a probe beam of 20-keV protons. The dissociation fraction was determined by measuring the decrease in the H^- signal produced by double electron capture from H_2 as the oven temperature is raised, and was measured to be 0.87 ± 0.03. This compares to a measured value of 0.92 ± 0.03 for the previous tube. The small decrease is due to the larger beam entrance aperture in the new tungsten tube, which increased the gas conductance from the tube, thereby increasing the probability for a hydrogen molecule to escape before dissociating. The target thickness was determined by normalization to well-known cross sections for single-electron-capture in $H^+ + H$ and $H^+ + H_2$ collisions.

The techniques for handling the target gas and procedures for reproducing a given target density are identical to those employed previously.[16,29,33] We use the gas-bypass technique described by Bayfield,[34] in which the same quantity of gas enters the vacuum system, whether it flows through the target cell during a cross-section signal measurement or bypasses the cell during a background measurement. The relative amount of gas flowing into the vacuum system is monitored by measuring the pressure drop across a copper capillary tube whose conductance is small compared to that of the gas cell apertures. This pressure drop can be measured reproducibly to $\pm1\%$ using a capacitance manometer, and under the molecular-flow conditions which prevailed in the experiments, was verified to bear an exact linear relationship to the quantity of gas admitted into the system. The target cell is differentially pumped by two liquid-nitrogen-trapped diffusion pumps having a net pumping speed of 2000 l/s. The operating pressure along the ion beam line was 2×10^{-4} Pa (1.5×10^{-6} Torr) or lower. Signal-to-background ratios varied typically in the range from 3:1 to 12:1, depending on the gas flow, the cross section being measured, and whether or not the oven tube was heated. For atomic-hydrogen cross-section measurements, corrections for undissociated H_2 in the target were made in the manner described previously,[33] and seldom exceeded 10%.

Measurements on H_2 and other gases are made by

operating the oven tube at room temperature. Some of the $C^{q+} + H_2$ electron-capture cross-section measurements reported here were measured using a different gas cell which was calibrated by a direct measurement of the quantity of gas flow into the target.[30] Cross-section measurements using the two collision cells are in excellent agreement.

Except for small changes which were ascribed to thermal expansion, the measured intensities of the low-energy ion beams from the laser source were essentially unaffected by the passage of 130 A through the oven tube. The cylindrical symmetry of the oven tube and of the supporting conductors through which the current was fed produce a cancellation of the magnetic field in the center of the tube.[35] It was found necessary, however, to bias the center of the oven tube at +10 V relative to ground, in order to suppress thermionic electron emission from the hot tungsten tube, and reduce the noise at the CEMA detector. This potential was taken into account when determining collision energies. The voltage drop across the tube was 4 V at the operating current of 130 A, and introduced a corresponding spread in collision energies which was observable only at the very lowest energies. A magnetic shield was placed between the oven and the nearest axial magnetic field coil at the higher energies, where larger fields were required to collimate the ion beam. This shield substantially reduced the field produced by the coils at the oven tube and eliminated some additional noise observed at the detector when the coils were pulsed. With the oven at 2350 K, a background count rate of roughly 1 kHz was observed at the detector under optimized conditions, and was attributed to photons from the oven tube. Measurement of both the count rate and the analog signal from the detector allowed its gain to be measured as a function of detector bias voltage.

Previous experience with the atomic-hydrogen target over several years of operation and more than one thousand heating cycles showed its calibration to remain constant and reproducible to better than 10%.[29,33] Several cross sections were remeasured at intervals during the course of these measurements in order to ascertain whether any detectable change in the target calibration had occurred. No such variations were detected outside the random uncertainties of these individual measurements (typically ±15% at 90% confidence level).

E. Cross-section measurement

Electron-capture cross sections were determined by measuring the fraction of ions which capture an electron as a function of the gas flow into the target cell, as described in Sec. II D. Under single-collision conditions, the variation of the net fraction (signal-minus-background) is linear, and the slope is proportional to the capture cross section. The time-of-flight technique permitted cross sections for several charge states q to be measured simultaneously, as illustrated in Fig. 2. A typical cross-section determination involved 10–30 repetitions of data like those shown in Fig. 2, from which the statistical reproducibility of the ratios could be assessed. Because the scattered signal and primary ion fluxes could be measured from the same laser shot, fluctuations in ion intensity did not contribute to the statistical uncertainty in the signal ratios. At the low gas densities used in this investigation, the variation of the growth of the net signal fraction with gas flow was verified to be linear for both the atomic- and molecular-hydrogen measurements, and the zero-gas-flow intercept was always consistent with zero within the statistical uncertainty, verifying the validity of the background subtraction procedure. The net signal fraction was varied between 1 and 10%. The relative effect of multiple collisions on the measurements was negligibly small, and could easly be detected and assessed in the time-of-flight spectra.

III. SYSTEMATICS AND UNCERTAINTIES

The systematic tests which were performed and the assessment of uncertainties in the measurements associated with the ORNL-PIG ion source have been discussed in detail.[16,29] Similar considerations for the time-of-flight experiments will be presented in this section.

The three major possible sources of uncertainty in the time-of-flight measurements were (a) the transmission through the deceleration section and the detection of all ions which entered the gas target cell; (b) the relative calibration of the detector for the signal and primary ions; and (c) the absolute calibration of the hydrogen target cell.

A. Ion collection

During the course of these measurements, more time was spent on systematic tests to verify complete ion collection than on the actual determinations of relative electron-capture signals. In order to temporally resolve the signal and primary ion fluxes, strong electrostatic deceleration was re-

quired, particularly for the highest q where $(q-1)/q$ approaches unity. Since any divergence in the beam is amplified in direct proportion to the change in axial velocity, much care was taken to assure that the field in the deceleration gap was axial. The axial magnetic field produced by the coils serves to counteract the blowup of the ion beam caused by deceleration. Prior to each cross-section measurement, the transmission through the deceleration section was measured for each charge q by comparing the ion signals obtained with no voltage applied to the deceleration tube and no current through the magnetic coils to that obtained with deceleration voltage and magnet current applied. The deceleration voltage was prescribed by the requirement of temporal resolution of the primary and signal ions, and the magnet current was made large enough to counteract ion beam blowup in the deceleration tube. The criterion established for making cross-section measurements was that the measured "transmission" for each charge q be in the range 1.0 ± 0.1. Such transmission measurements were sensitive to variations in the total ion flux, so that many iterations were necessary in order to obtain statistically significant measurements of intensity ratios. Small variations in sensitivity across the face of the CEMA made the measured "transmission" slightly larger than unity in some instances, as the ions were made to impact different areas of the detector surface. The axial magnetic field was always set to the minimum current necessary to ensure detection of all the ions, so as not to cause the beam to be focused to too small an area on the detector and cause a nonlinear response due to saturation.

The fact that the beam blowup due to electrostatic deceleration is less for the signal ions than for the primary ions by the ratio $(q-1)/q$, is offset by the fact that the primary beam is more strongly collimated by the magnetic field. Thus the primary and signal ions are expected to sample similar areas of the detector. Apparent cross sections were measured for several values of the axial magnetic field above the minimum necessary for total ion collection, and were found to be the same within the statistics of measurement. Caution was also taken to ensure that the beam divergence, which was controlled essentially by the einzel lens, did not exceed the $\pm2°$ angular acceptance of the target-cell apertures and the detector. Apparent cross sections measured with the einzel lens underfocused, and also with no potential applied were the same within statistics, indicating that angular scattering in the target cell did not cause a measurable loss of signal ions. The axial magnetic lens ensured that any signal ion which passed through the 2-mm target cell exit aperture would be detected. Careful consideration of these possible sources of error associated with transport of ions to the detector led to an estimated good-confidence uncertainty of $\pm9\%$ in the measured charge-exchange fraction. The term "good confidence" in this context refers to a level of confidence which is judged to be equivalent to 90% confidence level on statistical uncertainties. All systematic uncertainties in this paper are evaluated at this level.

B. Relative detector calibration

The CEMA detector itself contributed additional uncertainty to the measurements of the ratios of signal-to-primary ion fluxes. Since the CEMA was used in a current amplification mode, these ratios were sensitive to variations in sensitivity with ion-impact velocity and with ionic charge.

The linearity of the detector for the pulsed ion beam was initially determined *in situ* by measuring the transmission of a partially transparent fine-wire grid as a function of the CEMA gain. For a detector gain of 10^6 or lower, the transmission was measured to be 0.36 ± 0.05, which compares to an optical measurement of 0.30 ± 0.02. Additional measurements of charge-exchange fractions in relation to CEMA gain verified this result. Since the CEMA was used as current amplifier, the gain of the external preamplifier-amplifier was fixed at 160 based on these measurements, and the bias on the detector was adjusted such that the amplified signals did not saturate the 512-mV full-scale input of the transient digitizer. Despite variations in the ion fluxes, this permitted relatively uniform current pulses to be collected by the detector anode and recorded without concern about detector linearity. Periodic checks were made in order to verify the linearity of the detection system over the range of experimental conditions.

Since the CEMA front surface and grid were operated at negative high voltage, the primary ions of charge q were accelerated more strongly than the signal ions of charge $q-1$, and thus impacted the surface at a different energy. The arrangement of detector bias allowed *in situ* measurement of the variation of sensitivity with impact energy. A linear variation of sensitivity with impact energy was measured for C^{q+} ions ($q=2,3,4,5$) over the impact energy range 4–14 keV, and the slope was determined to be independent of charge. These

measurements were used to make a relative correction to the measured charge-exchange signal ion fluxes. Such corrections were smallest for the highest q, since $(q-1)/q$ approaches unity.

Possible variations in detector sensitivity with ionic charge q for ions of the same impact velocity were more difficult to assess. Such variations are expected to decrease as the velocity increases, and the mechanism for secondary electron ejection becomes predominantly kinetic rather than potential in nature.[36] Using the ORNL-PIG source, relative secondary-emission coefficients were measured for N^{q+} (q=2,3,4,5) ions incident on a CEMA surface at energies ranging from $2.5q$ to $10q$ keV. These measurements, along with relative measurement by Cano[37] for C^{q+} ions on gas-covered CuBe, Au, Mo, and Cu, and by Decoste and Ripin[38] for C^{q+} ions on Cu, were used to assess corrections for the intrinsic variation of secondary emission coefficient γ with ionic charge q. The measured ratios γ_q/γ_{q-1} were plotted versus energy for $q=3-6$, and in each case a median curve was drawn through the data in order to deduce relative corrections to the signal ion fluxes. Such corrections ranged from 10–30%, depending on the ionic charge and impact energy and decreased with increasing energy. The same corrections were applied for C^{q+} and O^{q+} ions. The uncertainty associated with this correction is estimated to be ±10% at good-confidence level.

C. Total uncertainties

The uncertainties associated with the calibration and implementation of the atomic-hydrogen target are similar to those described previously,[16,29,33] and are listed in Table I, along with the other uncertainties which have been discussed. Estimated total systematic uncertainties at good-confidence level sum in quadrature to ±22% and ±20% for time-of-flight measurements on atomic and molecular hydrogen, respectively. These compare to ±13.5% for the measurements made using the ORNL-PIG ion source and associated apparatus.[29]

IV. RESULTS AND DISCUSSION

The experimental electron-capture cross sections for collisions of C^{q+} and O^{q+} ions with H and H_2 are listed in Table II, along with the statistical

TABLE I. Summary of experimental uncertainties for time-of-flight measurements.

Source	$\sigma_{q,q-1}$ (H)	$\sigma_{q,q-1}$ (H_2)
Relative Ion Detection Efficiency:		
Angular distribution of scattered ions	± 5%	± 5%
Transmission through deceleration tube	± 9%	± 9%
Dependence of sensitivity on impact energy	±10%	±10%
Dependence of sensitivity on ionic charge	±10%	±10%
Detector linearity	± 3%	± 3%
Quadrature Sum	±18%	±18%
Gas-Target Calibration:		
Reproducibility of target thickness	± 6%	± 2%
Calibration (90% confidence level)		
Target gas purity (maximum effect on σ)	± 2%	± 2%
Reproducibility of gas flow	± 2%	± 2%
Uncertainty in dissociation fraction	± 4%	
Uncertainty in cross section used for normalization	±10%	±10%
Quadrature Sum	±13%	±10%
Total Absolute Uncertainty (Quadrature Sum)	±22%	±20%

reproducibility of each measurement at one standard deviation and the total absolute uncertainty estimated at good-confidence level. The latter represents the quadrature sum of the statistical uncertainty at 90% confidence level and total systematic uncertainties derived either as shown on Table I for the time-of-flight measurements (referred to as method 1), or from Ref. 29 for the measurements made using the ORNL-PIG source (method 2). The data for H_2 refer to capture of a single electron only. Although the ranges of energies for the two methods are generally contiguous, there is an actual overlap only in the cases of the $O^{3+} + H_2$ and $O^{4+} + H_2$ measurements. In all cases the data obtained using these two methods are consistent within the total uncertainties, or join smoothly together. Some of the time-of-flight measurements for $C^{q+} + H_2$ collisions have been published in brief reports.[30,39] The data in those publications, however, were uncorrected for variations in detector sensitivity with ionic charge, as discussed in Sec. III. Thus the present values supersede those plotted in Refs. 30 and 39.

The ranges of energies for which measurements were made using the laser ion source reflect the availability of adequate fluxes of ions of the various charges q from the laser-produced plasma, and the ability to resolve the signal and primary ions by the time-of-flight technique. In the case of the measurements made using the ORNL-PIG ion source, the ability to extract ions from the magnetically confined discharge set the lower energy limit on the measurements.

A. $C^{6+} + H$, $O^{6+} + H$ systems

From a basic physics perspective, the $C^{6+} + H$ cross-section measurements are the most significant. This one-electron diatomic system is the simplest from a theoretical point of view, and has con-

TABLE II. Experimental electron-capture cross sections.

Ion	Energy (eV/amu)	Velocity (10^7 cm/s)	$\sigma_{q,q-1}(H)$	Standard deviation (10^{-16} cm^2)	Absolute uncertainty	$\sigma_{q,q-1}(H_2)$	Standard deviation (10^{-16} cm^2)	Absolute uncertainty	Method
O^{2+}	188	1.90	4.1	0.3	0.8	1.2	0.3	0.6	2
	375	2.69	2.5	0.2	0.5	1.8	0.1	0.3	2
	656	3.56	1.9	0.1	0.3	2.2	0.2	0.5	2
	1255	4.92	2.2	0.1	0.4	2.9	0.1	0.4	2
	1885	6.04	2.0	0.1	0.3	3.1	0.1	0.5	2
	2520	6.98	2.3	0.1	0.4	3.8	0.1	0.6	2
	3275	7.95	3.3	0.3	0.7	3.9	0.1	0.6	2
O^{3+}	42	0.90	29.8	5.6	11.6				1
	61	1.08				23.7	1.3	5.2	1
	73	1.19	34.6	6.0	12.7				1
	193	1.93	31.7	4.2	10.0	20.9	2.2	5.6	1
	281	2.33	23.2	0.7	3.4	9.4	0.4	1.5	2
	363	2.65				7.7	3.2	5.7	1
	563	3.30	25.3	3.6	8.0	8.3	0.2	1.2	2
	983	4.35	26.7	0.6	3.8	8.6	0.3	1.3	2
	1890	6.03	23.7	0.4	3.3	9.6	0.4	1.5	2
	2830	7.39	22.6	0.5	3.2	9.9	0.3	1.5	2
	3770	8.53	21.8	0.5	3.1	11.3	0.5	1.8	2
	4915	9.74	22.4	1.3	4.0	11.7	0.6	2.0	2
O^{4+}	56	1.04	25.3	5.0	10.2				1
	81	1.25				41.0	3.5	10.1	1
	98	1.37	33.9	3.8	9.9				1
	128	1.57	39.6	3.5	10.5	38.0	3.1	9.2	1
	215	2.04	30.5	3.2	8.6				1
	257	2.23	26.6	3.7	8.6	39.6	6.4	13.5	1
	323	2.49				35.1	3.6	9.3	1
	375	2.69	23.3	0.9	3.6	25.5	0.4	3.5	2

TABLE II. (*Continued.*)

Ion	Energy (eV/amu)	Velocity (10^7 cm/s)	$\sigma_{q,q-1}$(H)	Standard deviation (10^{-16} cm^2)	Absolute uncertainty	$\sigma_{q,q-1}(H_2)$	Standard deviation (10^{-16} cm^2)	Absolute uncertainty	Method
	484	3.05				35.8	3.3	9.1	1
	750	3.80	26.3	0.8	3.9	27.0	0.8	4.0	2
	1310	5.03	28.3	1.2	4.5	32.2	0.7	4.6	2
	2515	6.97	26.9	1.4	4.6	29.8	0.9	4.4	2
	3775	8.53	24.4	1.0	3.9	28.4	0.7	4.1	2
	5050	9.87	24.5	0.3	3.4	26.2	0.7	3.8	2
	6575	11.26	23.3	0.7	3.4	25.5	0.3	3.5	2
O^{5+}	69	1.16	64.1	3.3	15.2				1
	100	1.39	71.8	6.8	19.6	18.5	3.9	7.6	1
	122	1.53	64.0	5.0	16.4				1
	160	1.76	55.8	5.8	15.7	22.4	4.6	9.0	1
	219	2.06	57.7	4.5	14.8				1
	269	2.28	37.7	3.4	10.1				1
	320	2.48	32.5	2.8	8.6	18.8	5.5	10.1	1
	403	2.79				19.5	2.6	5.9	1
	605	3.41				23.1	4.1	8.4	1
	938	4.25	35.8	0.8	5.1	16.8	0.4	2.4	2
	1630	5.61	33.8	0.4	4.6	19.6	0.4	2.8	2
	3135	7.78	34.5	4.5	10.1	22.0	0.8	3.4	2
	4720	9.54	33.6	1.1	5.0	22.7	0.5	3.2	2
	6310	11.04	34.5	1.7	5.8	23.2	0.4	3.2	2
	8205	12.58	33.5	1.3	5.2	25.7	1.2	4.2	2
O^{6+}	83	1.27	25.0	2.5	7.0				1
	120	1.52	27.0	2.4	7.2	52.4	2.9	11.6	1
	145	1.67				55.1	4.0	12.9	1
	169	1.81				50.4	7.0	15.6	1
	192	1.92	36.5	2.9	9.4	51.2	5.2	13.5	1
	264	2.26	36.7	2.3	9.0	49.1	1.6	10.2	1
	323	2.50	42.1	2.0	9.9				1
	383	2.72	36.5	4.1	10.6				1
	484	3.05				51.8	4.5	12.9	1
	726	3.74				47.9	2.8	10.7	1
	1125	4.66	31.1	1.5	5.2	41.4	1.4	6.3	2
	1975	6.17	37.0	0.8	5.2	39.8	0.5	5.5	2
	3760	8.52	37.9	2.0	6.5	38.6	1.0	5.6	2
	5675	10.46	39.7	2.6	7.5	37.0	1.2	5.5	2
	7540	12.06	40.2	1.1	5.9	37.2	0.4	5.1	2
	9860	13.80	41.8	0.5	5.7	37.7	0.9	5.4	2
C^{3+}	11	0.46	14.7	2.0	4.7	8.0	2.1	3.9	1
	20	0.62	10.0	1.2	3.1	9.4	0.7	2.2	1
	36	0.84	8.5	1.2	2.7				1
	39	0.87				13.1	1.5	3.7	1
	43	0.91	7.5	0.7	2.0				1
	57	1.04				11.6	1.1	3.0	1
	70	1.16	6.8	0.9	2.1	10.2	1.0	2.7	1
	112	1.47	6.2	1.6	3.0	9.0	1.2	2.7	1
	161	1.76				5.6	1.6	2.9	1
C^{4+}	15	0.54	13.7	3.2	6.3				1
	27	0.72	17.0	2.9	6.3	53.2	4.9	13.5	1
	50	0.98	22.8	2.3	6.3	55.6	4.5	13.5	1

TABLE II. (*Continued.*)

Ion	Energy (eV/amu)	Velocity (10^7 cm/s)	$\sigma_{q,q-1}(H)$	Standard deviation (10^{-16} cm^2)	Absolute uncertainty	$\sigma_{q,q-1}(H_2)$	Standard deviation (10^{-16} cm^2)	Absolute uncertainty	Method
	57	1.05	20.9	1.6	5.4				1
	75	1.20				44.5	1.7	9.4	1
	93	1.34	23.2	1.0	5.4	43.6	0.5	8.8	1
	150	1.70	25.0	1.1	5.5	37.3	2.8	8.8	1
	214	2.03	21.2	1.3	5.2	35.6	0.9	7.3	1
	387	2.73	32.7	1.9	7.9	39.1	2.3	8.7	1
C^{5+}	71	1.17	24.9	3.7	8.4				1
	94	1.35				20.4	0.9	4.4	1
	115	1.49	24.4	2.1	6.5	21.6	2.7	6.3	1
	186	1.90	20.3	2.4	6.1	14.5	1.7	4.1	1
	268	2.27	22.1	1.7	5.7	8.5	0.5	1.9	1
	2490	6.93	27.2	0.8	4.0	17.9	0.5	2.6	2
	4280	9.09	31.2	1.3	4.9	23.5	0.8	3.6	2
	8750	12.99	36.4	1.0	5.3	28.8	0.4	4.0	2
C^{6+}	142	1.66	7.0	3.8	5.6	34.1	4.3	10.0	1
	160	1.74	11.8	2.6	5.1	38.4	4.4	10.7	1
	221	2.06	17.8	3.2	6.3				1
	319	2.47	30.7	3.2	8.7	48.0	5.7	13.6	1

sequently received the most attention. The present measurements, along with data of Goffe *et al.*,[40] taken at much higher energies, are compared to the available theory in Fig. 3. The present data at 160 and 319 eV/amu are new measurements which were not reported in Ref. 28. The present data are consistent with the PSS impact-parameter calculations of Salop and Olson[19] (6-state) and of Green *et al.*[24] (33-state), but exceed that of Vaaben and Briggs[20] (11-state) at the higher energies. The 4-state fully quantal calculation of Bottcher and Heil[26] underestimates the measurements at the lower energies, but the inclusion of a larger number of coupled states is expected to increase the cross section in this region. The unitarized-distorted-wave calculation of Ryufuku and Watanabe[27] significantly overestimates the cross section in this region, but essentially converges to the classical trajectory Monte Carlo calculation of Salop and Olson[19] at energies above a few keV/amu. The classical calculation gives the best agreement with the high-energy data of Goffe *et al.*[40]

The $O^{6+}+H$ cross section is not characterized by as precipitous a fall-off with decreasing energy as is the case for $C^{6+}+H$. In Fig. 4, present $O^{6+}+H$ measurements are compared to experimental data of Crandall *et al.*[29] and Gardner *et al.*,[41] and to the 6-state PSS calculation of Shipsey *et al.*[42] Also plotted for comparison are the $C^{6+}+H$ measurements and the theory of Green *et al.*,[24] which is considered to be the most definitive. The $O^{6+}+H$ calculation predicts a weaker velocity dependence than for the fully stripped case, but generally overestimates the measured cross sections, particularly at the lowest energies. The data do suggest the predicted local maximum in the cross section, but at somewhat lower energy. For both systems, the calculations indicate that the $n=4$ final states of the five-times-ionized ion are dominant at energies of a few keV/amu and below. This suggests that the difference in the behavior of the cross sections at lower velocities is due to the effect of the additional bound ionic electron on the coupling in the O^{6+} case. A similar, but much larger effect is evident in the comparison of the $C^{5+}+H$ and $O^{5+}+H$ cross sections. The disagreement with the measurements of Gardner *et al.* is attributed to procedures used for calibration of the atomic-hydrogen target, and has been discussed previously.[29]

B. $C^{5+}+H$, $O^{5+}+H$ systems

The present measurements for $C^{5+}+H$ and $O^{5+}+H$ are plotted in Fig. 5, along with other published data[29,41] and the PSS calculations of Shipsey *et al.*[42] and Bottcher and Heil[26] for the C^{5+}

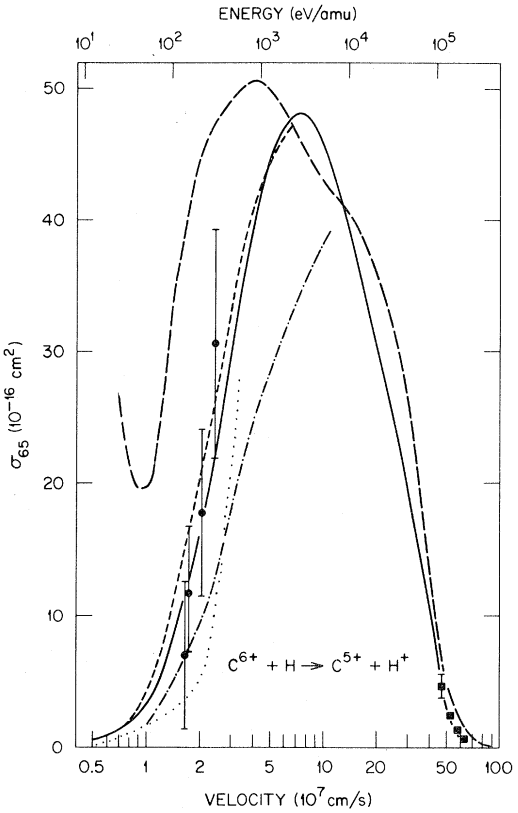

FIG. 3. Electron-capture cross sections for $C^{6+} + H$ collisions. Circles are present experimental results and error bars are estimated total experimental uncertainties at good confidence level. Squares are data of Goffe *et al.* (Ref. 40). Solid curve is PSS calculation joined to classical trajectory Monte Carlo calculation at higher energy, from Salop and Olson (Ref. 19). Short-dashed, dot-dashed, and dotted curves are PSS calculations of Green *et al.* (Ref. 24), Vaaben and Briggs (Ref. 20), and Bottcher and Heil (Ref. 26), respectively. Long-dashed curve is distorted-wave calculation of Ryufuku and Watanabe (Ref. 27).

case. As is the case for the 6+ ions, production of the $n=4$ levels of C^{4+} dominates the electron-capture cross section, with only a very small contribution to $n=3$ levels. Theory and experiment are in reasonable agreement in this case. The O^{5+} cross section shows a large enhancement at decreasing energy below 200 eV/amu, and in fact exceeds the C^{5+} cross section by a factor of 2–3 at 100 eV/amu. Such behavior is indicated in preliminary quantal PSS calculations by Bottcher and Heil,[43] and is attributed to velocity-dependent variations in the coupling between the molecular states of OH^{5+} which dissociate into O^{4+} $(n=4) + H^+$ at large distances. We are not aware of any specific calculations in the literature for low-energy $O^{5+} + H$ electron-capture collisions.

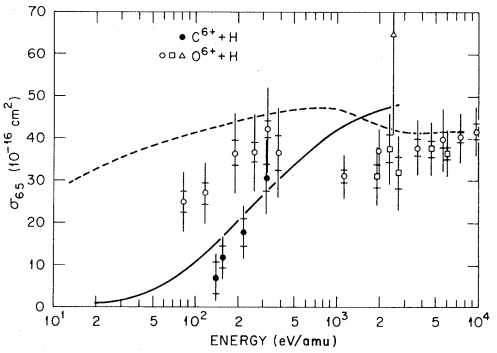

FIG. 4. Electron-capture cross sections for $C^{6+} + H$ (solid points and solid curve) and $O^{6+} + H$ (open points and dashed curve). Circles are present data, with inner and outer error bars denoting statistical and estimated total experimental uncertainties, as listed in Table II. Squares are experimental data of Crandall *et al.* (Ref. 29), and triangle is measurement of Gardner *et al.* (Ref. 41). Solid and dashed curves are PSS calculations of Green *et al.* (Ref. 24) for $C^{6+} + H$ and of Shipsey *et al.* (Ref. 42) for $O^{6+} + H$, respectively.

C. $C^{4+} + H$, $O^{4+} + H$ systems

Experimental electron-capture cross sections for $O^{4+} + H$ and $C^{4+} + H$ collisions are plotted in Fig. 6, along with the PSS calculations of Bottcher and Heil,[26] Olson *et al.*,[44] and Gargaud *et al.*[45] for the

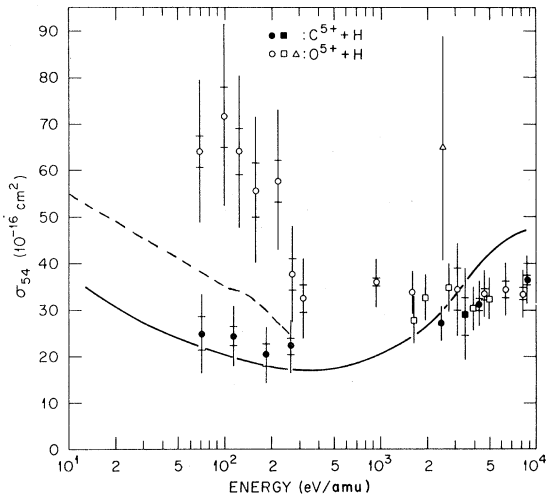

FIG. 5. Electron-capture cross sections for $C^{5+} + H$ (solid points and curves) and $O^{5+} + H$ (open points). Symbols are defined as in Fig. 4, solid curve is PSS calculation of Shipsey *et al.* (Ref. 42), and dashed curve is PSS calculation of Bottcher and Heil (Ref. 26).

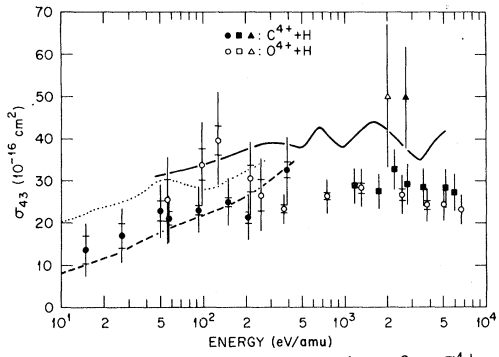

FIG. 6. Electron-capture cross sections for $C^{4+} + H$ (solid points and curves) and $O^{4+} + H$ (open points). Symbols are as defined in Fig. 4. Solid, dashed, and dotted curves are PSS calculations for $C^{4+} + H$ of Olson *et al.* (Ref. 44), of Gargaud *et al.* (Ref. 45), and of Bottcher and Heil (Ref. 26), respectively.

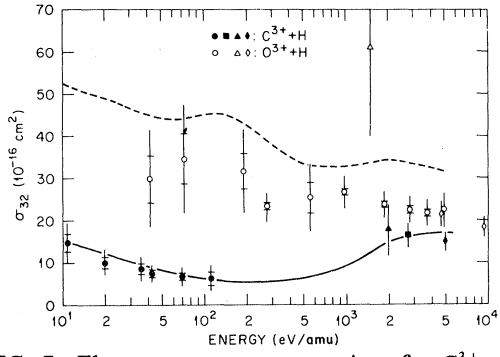

FIG. 7. Electron-capture cross sections for $C^{3+} + H$ (solid points and solid curve) and $O^{3+} + H$ (open points and dashed curve). Circles are present experimental data, and diamonds, triangles, and the square are measurements of Phaneuf *et al.* (Ref. 33), Gardner *et al.* (Ref. 41), and Crandall *et al.* (Ref. 29), respectively. Solid and dashed curves are PSS calculations of Bienstock *et al.* from Refs. 46 and 47, respectively.

C^{4+} case. The agreement between the present results and the theory of Gargaud *et al.*[45] is considered excellent. Both Gargaud *et al.* and Bottcher and Heil employ a fully quantum-mechanical treatment of the collision dynamics, which should be more reliable at the lowest velocities than the straight-line-trajectory approach used by Olson *et al.* The methods appear to converge above 500 eV/amu. Except for a "bump" in the O^{4+} cross section in the 100—150 eV/amu energy range, the C^{4+} and O^{4+} cross sections are almost indistinguishable experimentally over the $10-10^4$-eV/amu energy range. Perhaps coincidentally, this feature occurs at roughly the same energy as the large enhancement observed in the O^{5+} case. The increasing quantitative similarity in electron-capture cross sections for multiply charged ions of the same charge, as the number of electrons on the ion increases, is an expected result.[16] In the $C^{4+} + H$ system, curve crossings between molecular states which correlate to $n = 3$ final states are dominant,[45] and a similar situation is expected for O^{4+}.

D. $C^{3+} + H$, $O^{3+} + H$ systems

Present experimental data for $C^{3+} + H$ and $O^{3+} + H$ systems are compared in Fig. 7 to other measurements,[33,41] and to recent fully quantal PSS calculations Bienstock *et al.*[46,47] The agreement is excellent in the C^{3+} case over the entire energy range. The $O^{3+} + H$ calculation is consistent with the observed energy dependence, but uniformly exceeds the data by about 30%. Whereas there are no metastable states for Li-like C^{3+}, it is probable that a finite fraction of B-like O^{3+} ion beam is in the $(1s^2 2s\,2p^2)^4P$ metastable state, for which the curve crossings may be less favorable for electron capture. Measurements of cross sections for electron-impact ionization of O^{3+} ions[48] obtained from the same ORNL-PIG source used for some of these measurements indicated a metastable ion content of 16%. A similar relative abundance would be expected from the laser-produced plasma. Were the cross section to be negligible for metastable $O^{3+}(^4P)$ incident ions, the disagreement with theory could be partially reconciled.

E. Molecular-hydrogen results

Present measurements for $C^{q+} + H_2$ and $O^{q+} + H_2$ collisions are plotted along with other published data[29,49–51] in Figs. 8 and 9. The consistency between the various measurements is satisfying. For both carbon and oxygen ions the cross sections for incident charge $q = 4$ are larger than those for $q = 5$ at low energy. This phenomenon has been attributed to the relatively larger abundance of curve crossings leading to product excited levels with lower principal quantum number ($n \leq 3$) for $q = 4$ systems.[51] Corresponding cross sections for collisions with atomic hydrogen do not show this behavior. No apparent uniformities in the relative magnitudes of the cross sections for atomic and molecular hydrogen targets are suggested by the present data. This contrasts the situation at ener-

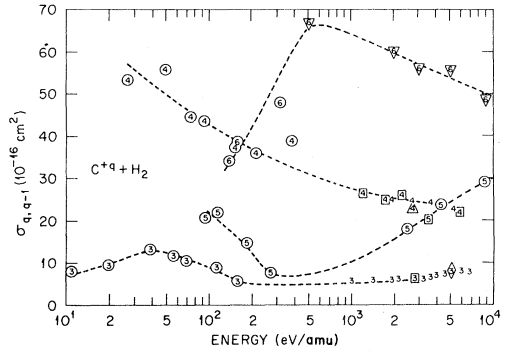

FIG. 8. Experimental electron-capture cross sections for $C^{q+} + H_2$ collisions. Numbers designate initial ionic charge q. Circles are present data, squares are measurements of Crandall *et al.* (Ref. 29), triangles are from Gardner *et al.* (Ref. 50), inverted triangles for $q = 6$ are from Afrosimov *et al.* (Ref. 49), diamonds are from Phaneuf *et al.* (Ref. 33), and numbers without symbols are from Crandall *et al.* (Ref. 51). Several data points from these references are not plotted, where measurements are overlapping. Curves are drawn for clarity only.

gies of 50 keV/amu and above, where such electron-capture cross sections for H_2 exceed those for H atoms by factors of 2—3.[33] In this higher energy range, the cross sections are also observed to increase monotonically with ionic charge q, approximately as q^p, where the power p varies between 1 and 3, and increases with collision energy.[33,52]

F. Summary

Electron-capture cross sections for highly stripped carbon and oxygen ions colliding with hydrogen atoms and molecules at low energy (< 10 keV/amu) are observed neither to obey simple charge-scaling rules, nor to be characterized by a

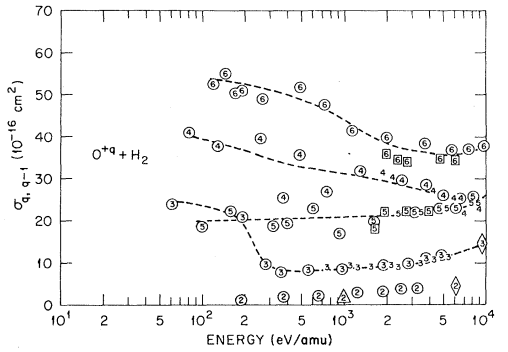

FIG. 9. Experimental electron-capture cross sections for $O^{q+} + H_2$ collisions. Symbols are defined as in Fig. 8. Curves are drawn for clarity only.

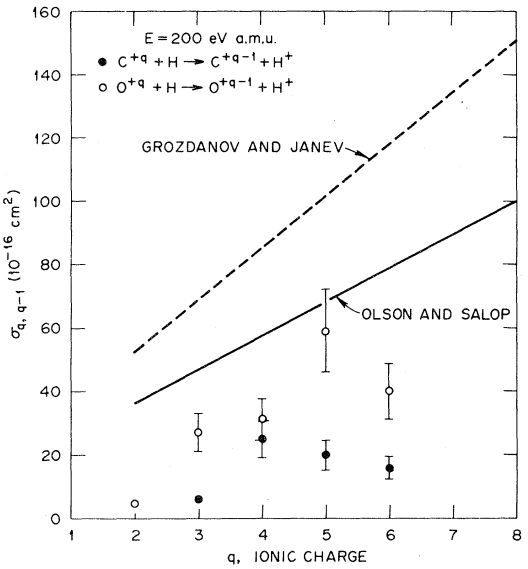

FIG. 10. Present electron-capture cross sections for $C^{q+} + H$ collisions (solid points) and $O^{q+} + H$ collisions (open points), plotted versus initial ionic charge q, for a fixed collision energy of 200 eV/amu. Dashed curve is based on tunnelling model of Grozdanov and Janev (Ref. 12), and solid curve is absorbing-sphere model of Olson and Salop (Ref. 9).

specific dependence on collision velocity. The lack of any charge scaling is illustrated in Fig. 10, where the present cross-section measurements for $C^{q+} + H$ and $O^{q+} + H$ collisions are plotted versus ionic charge q at a fixed collision energy of 200 eV/amu. Also plotted are calculations based on the absorbing-sphere model of Olson and Salop,[9] and the tunnelling model of Grozdanov and Janev,[12] both of which predict a linear variation with q over this range, and predict cross sections which significantly exceed the measurements. Also noteworthy is the fact that for each charge q, the cross sections for oxygen ions exceed those for carbon ions at 200 eV/amu, with a mean ratio of 2.8 ± 1.4. This is consistent with an earlier analysis of data at 830 eV/amu by Crandall *et al.*[16] The cross sections for a wide variety of ions of fixed q colliding with atomic hydrogen were observed to increase with the number of bound electrons on the incident ion, with an apparent saturation for 10—20 bound electrons. This is attributed in part to the effect of the bound electrons on the coupling between the levels involved, and in part to the increase in the number of favorable curve-crossings which are available for charge transfer to occur.

For those systems where detailed perturbed-

stationary-state calculations employing a molecular basis have been performed, the agreement with the present experimental data is considered to be good, both with respect to the magnitude of the cross section and to its velocity dependence. As expected, the best agreement with experiment at low energies is obtained by those calculations in which both the collision dynamics and the intermolecular coupling are treated quantum mechanically.[45–47]

ACKNOWLEDGMENTS

The authors are indebted to C. F. Barnett for proposing the laser experiments and for encouragement. They are also grateful to J. A. Hale for rendering continuing valuable technical assistance. R. H. Hughes suggested and designed the magnetic field coils for the deceleration section, and contributed to many helpful discussions while on leave from the University of Arkansas. D. P. Hutchinson was most helpful in providing advice concerning the implementation of the CO_2 laser. Special thanks are due C. Bottcher, T. G. Heil, T. A. Green, R. E. Olson, and R. McCarroll for discussions which provided physical insight, and for communicating theoretical results prior to publication. This research was supported in part by the Office of Basic Energy Sciences, and in part by the Office of Fusion Energy, U.S. Department of Energy under Contract No. W-7405-eng-26 with the Union Carbide Corporation. I. Alvarez acknowledges support from COMACYT under Contract No. 10 PMBC 790082.

*Permanent address: Institute of Physics, Universidad Nacional Autonoma de Mexico, Mexico 20-364.

[1]R. McCray, C. Wright, and S. J. Hatchett, Astrophys. J. 211, L29 (1977).
[2]R. B. Christensen, W. D. Watson, and R. J. Blint, Astrophys. J. 213, 712 (1977).
[3]H. W. Drawin, Phys. Scr. 24, 622 (1981).
[4]R. A. Hulse, D. E. Post, and D. R. Mikkelsen, J. Phys. B 13, 3895 (1980).
[5]R. C. Isler, L. E. Murray, S. Kasai, J. L. Dunlap, S. C. Bates, P. H. Edmonds, E. A. Lazarus, C. H. Ma, and M. Murakami, Phys. Rev. A 24, 2701 (1981).
[6]R. C. Isler and E. C. Crume, Phys. Rev. Lett. 41, 1296 (1978).
[7]V. V. Afrosimov, Yu. S. Gordeev, A. N. Zinov'ev, and A. A. Korotkov, Pis'ma Zh. Eksp. Teor. Fiz. 28, 540 (1978) [JETP Lett. 28, 500 (1978)].
[8]J. Arianer, IEEE Trans. Nucl. Sci. NS-28, 1018 (1981).
[9]R. E. Olson and A. Salop, Phys. Rev. A 14, 579 (1976).
[10]L. P. Presnyakov and A. D. Ulantsev, Kvant. Elektron. (Moscow) 1, 2377 (1974) [Sov. J. Quantum Electron. 4, 1320 (1975)].
[11]M. I. Chibisov, Pis'ma Zh. Eksp. Teor. Fiz. 24, 56 (1976) [JETP Lett. 24, 46 (1976)].
[12]T. P. Grozdanov and R. K. Janev, Phys. Rev. A 17, 880 (1978).
[13]H. Klinger, A. Müller, and E. Salzborn, J. Phys. B 8, 230 (1975).
[14]S. Bliman, S. Dousson, B. Jacquot, and D. Van Houtte, J. Phys. (Paris) 42, 1387 (1981).
[15]E. Justiniano, C. L. Cocke, T. J. Gray, R. Du Bois, and C. Can, Phys. Rev. A 24, 2953 (1981).
[16]D. H. Crandall, R. A. Phaneuf, and F. W. Meyer, Phys. Rev. A 22, 379 (1980).
[17]S. Bliman, J. Aubert, R. Geller, B. Jacquot, and D. Van Houtte, Phys. Rev. A 23, 1703 (1981).
[18]R. E. Olson, in *Proceedings of the Eleventh ICPEAC, Kyoto, 1979,* edited by N. Oda and K. Takayanagi (North-Holland, Amsterdam, 1980), pp. 391–405.
[19]A. Salop and R. E. Olson, Phys. Rev. A 16, 1811 (1977).
[20]J. Vaaben and J. S. Briggs, J. Phys. B 10, L521 (1977).
[21]C. Harel and A. Salin, J. Phys. B 10, 3511 (1977).
[22]P. T. Greenland, J. Phys. B 11, L191 (1978).
[23]D. S. F. Crothers and N. R. Todd, J. Phys. B 13, 547 (1980).
[24]T. A. Green, E. J. Shipsey, and J. C. Browne, Phys. Rev. A 23, 546 (1981); 25, 1364 (1982).
[25]T. G. Heil, S. E. Butler, and A. Dalgarno, Phys. Rev. A 23, 1100 (1981).
[26]C. Bottcher and T. G. Heil, Chem. Phys. Lett. 86, 506 (1982).
[27]H. Ryufuku and T. Watanabe, Phys. Rev. A 19, 1538 (1979).
[28]R. A. Phaneuf, Phys. Rev. A 24, 1138 (1981).
[29]D. H. Crandall, R. A. Phaneuf, and F. W. Meyer, Phys. Rev. A 19, 504 (1979).
[30]R. A. Phaneuf, IEEE Trans. Nucl. Sci. NS-28, 1182 (1981).
[31]J. Goldhar, R. Mariella, Jr., and A. Javan, Appl. Phys. Lett. 29, 96 (1976).
[32]J. A. Ray and C. F. Barnett, IEEE Trans. Nucl. Sci. NS-17, 44 (1970).
[33]R. A. Phaneuf, F. W. Meyer, and R. H. McKnight, Phys. Rev. A 17, 534 (1978).
[34]J. E. Bayfield, Phys. Rev. 182, 115 (1969).
[35]G. W. McClure, Phys. Rev. 148, 47 (1966).
[36]K. H. Krebs, Fortschr. Phys. 16, 419 (1968).
[37]G. L. Cano, J. Appl. Phys. 44, 5293 (1973).
[38]R. Decoste and B. H. Ripin, NRL Memorandum Report No. 3814, Naval Research Laboratory, Washington, D.C. (unpublished).
[39]R. A. Phaneuf, D. H. Crandall, and F. W. Meyer, Phys. Scr. 23, 188 (1981).
[40]T. V. Goffe, M. B. Shah, and H. B. Gilbody, J. Phys. B 12, 3763 (1979).

[41]L. D. Gardner, J. E. Bayfield, P. M. Koch, I. A. Sellin, D. J. Pegg, R. S. Peterson, and D. H. Crandall, Phys. Rev. A 21, 1397 (1980).
[42]E. J. Shipsey, J. C. Browne, and R. E. Olson, J. Phys. B 14, 869 (1981).
[43]C. Bottcher and T. G. Heil, private communication.
[44]R. E. Olson, E. J. Shipsey, and J. C. Browne, J. Phys. B 11, 699 (1978).
[45]M. Gargaud, J. Hanssen, R. McCarroll, and P. Valiron, J. Phys. B 14, 2259 (1981).
[46]S. Bienstock, T. G. Heil, C. Bottcher, and A. Dalgarno, Phys. Rev. A 25, 2850 (1982).
[47]S. Bienstock, T. G. Heil, and A. Dalgarno, private communication.
[48]D. H. Crandall, R. A. Phaneuf, and D. C. Gregory, Report No. ORNL/TM-7020 (unpublished).
[49]V. V. Afrosimov, A. A. Basaleev, E. D. Donets, K. O. Lozhkin, and M. N. Panov, Pis'ma Zh. Eksp. Teor. Fiz. 34, 179 (1981) [JETP Lett. 34, 171 (1981)].
[50]L. D. Gardner, J. E. Bayfield, P. M. Koch, I. A. Sellin, D. J. Pegg, R. S. Peterson, M. L. Mallory, and D. H. Crandall, Phys. Rev. A 20, 766 (1979).
[51]D. H. Crandall, M. L. Mallory, and D. C. Kocher, Phys. Rev. A 15, 61 (1977).
[52]F. W. Meyer, R. A. Phaneuf, H. J. Kim, P. Hvelplund, and P. H. Stelson, Phys. Rev. A 19, 515 (1979).